Electronic Supplementary Information for

Intermetallic $Cu_{11}In_9$ In-Situ Formed on Hierarchical Nanoporous Cu for Highly Selective CO_2 Electroreduction

Wu-Bin Wan[‡a], Tian-Yi Dai[‡a], Hang Shi[‡a], Shu-Pei Zeng[a], Zi Wen[a], Wei Zhang[a], Xing-You Lang[a,b,*], Qing Jiang[a,*]

[a] *Key Laboratory of Automobile Materials (Jilin University), Ministry of Education, and School of Materials Science and Engineering, Jilin University, Changchun 130022, China*

[b] *State Key Laboratory of Automotive Simulation and Control, Jilin University, 130022 Changchun, China*

‡ These authors contributed equally to this work.
*Corresponding author.
E-mail: xylang@jlu.edu.cn (X.Y. Lang),
jiangq@jlu.edu.cn (Q. Jiang).

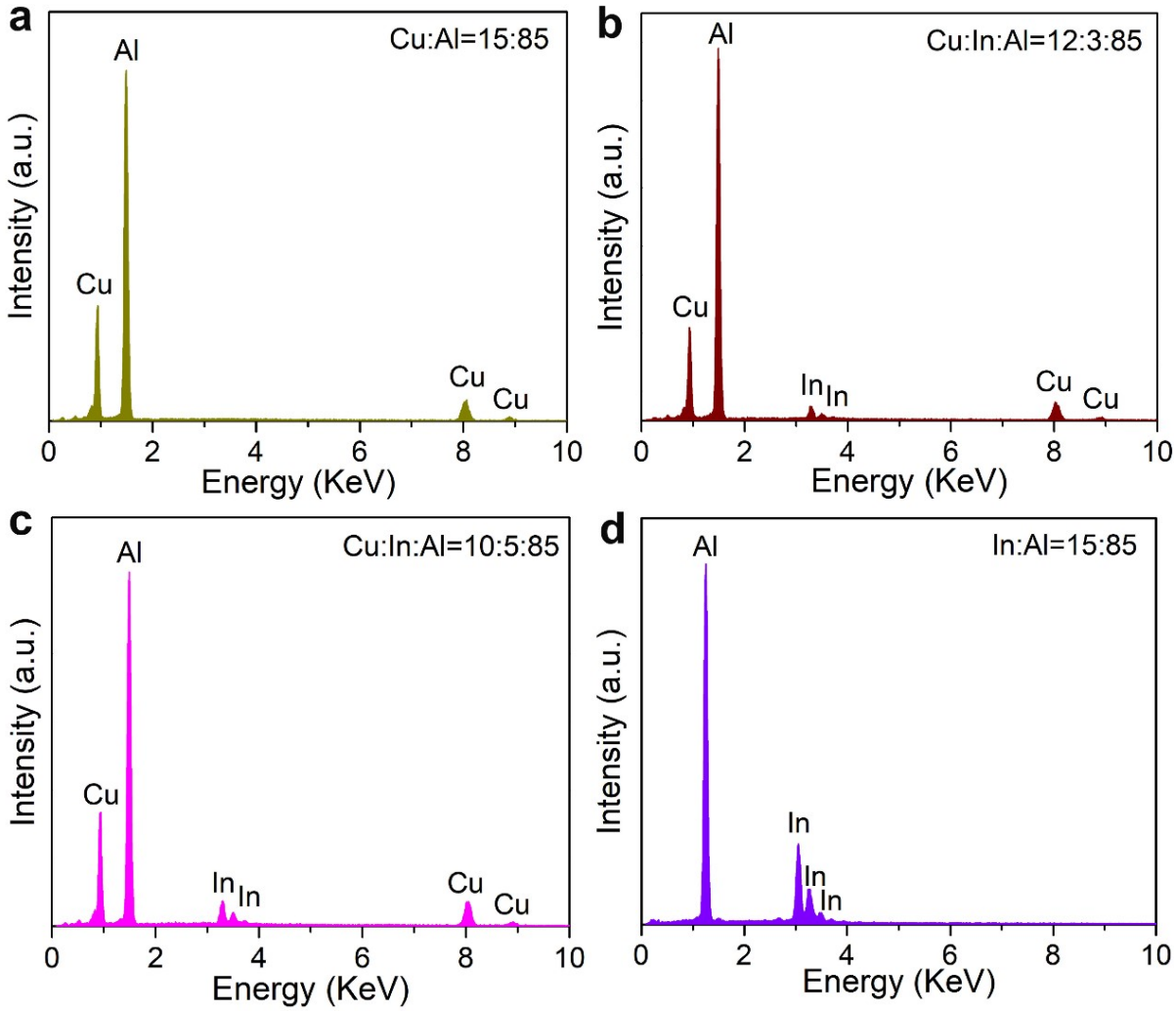

Fig. S1. EDS spectra of precursor $Cu_{15-x}In_xAl_{85}$ alloys. (a) EDS spectrum of $Cu_{15}Al_{85}$ alloy. (b) EDS spectrum of $Cu_{12}In_3Al_{85}$ alloy. c, EDS spectrum of $Cu_{10}In_5Al_{85}$ alloy. d, EDS spectrum $In_{15}Al_{85}$ alloy.

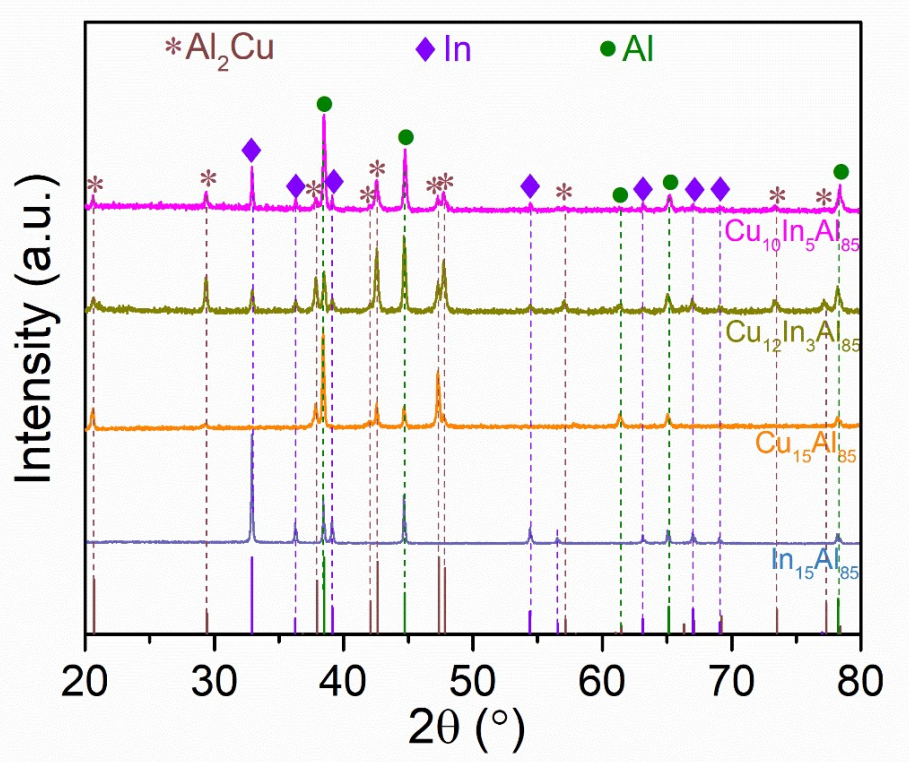

Fig. S2. XRD patterns of precursor alloys of $Cu_{15-x}In_xAl_{85}$ alloys with x = 0, 3, 5 and 15.

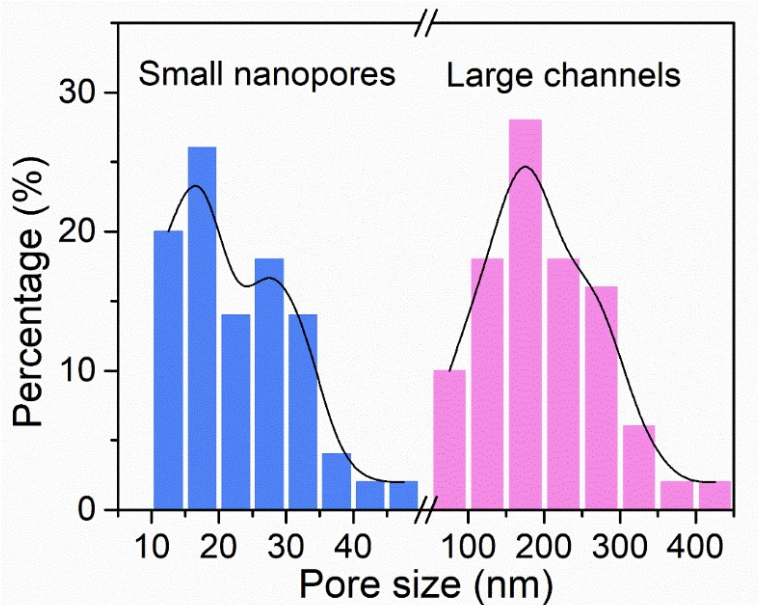

Fig. S3. Size distribution of small nanopores and large channels in hierarchical nanoporous $Cu_{11}In_9$/Cu hybrid electrode that is fabricated by chemically dealloying $Cu_{10}In_5Al_{85}$ precursor alloy.

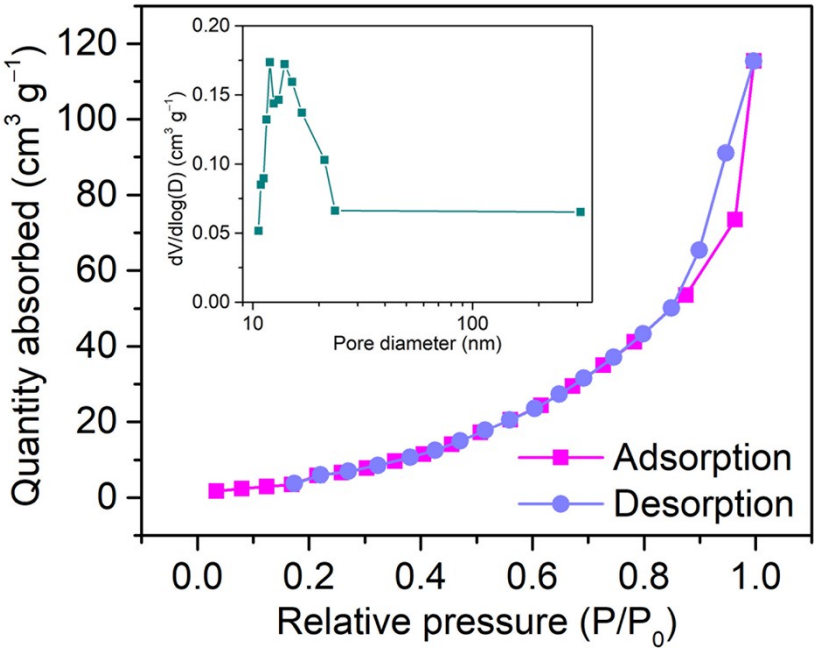

Fig. S4. The nitrogen adsorption/desorption isotherm of nanoporous $Cu_{11}In_9$/Cu hybrid electrode. Inset: Size distribution of small nanopores.

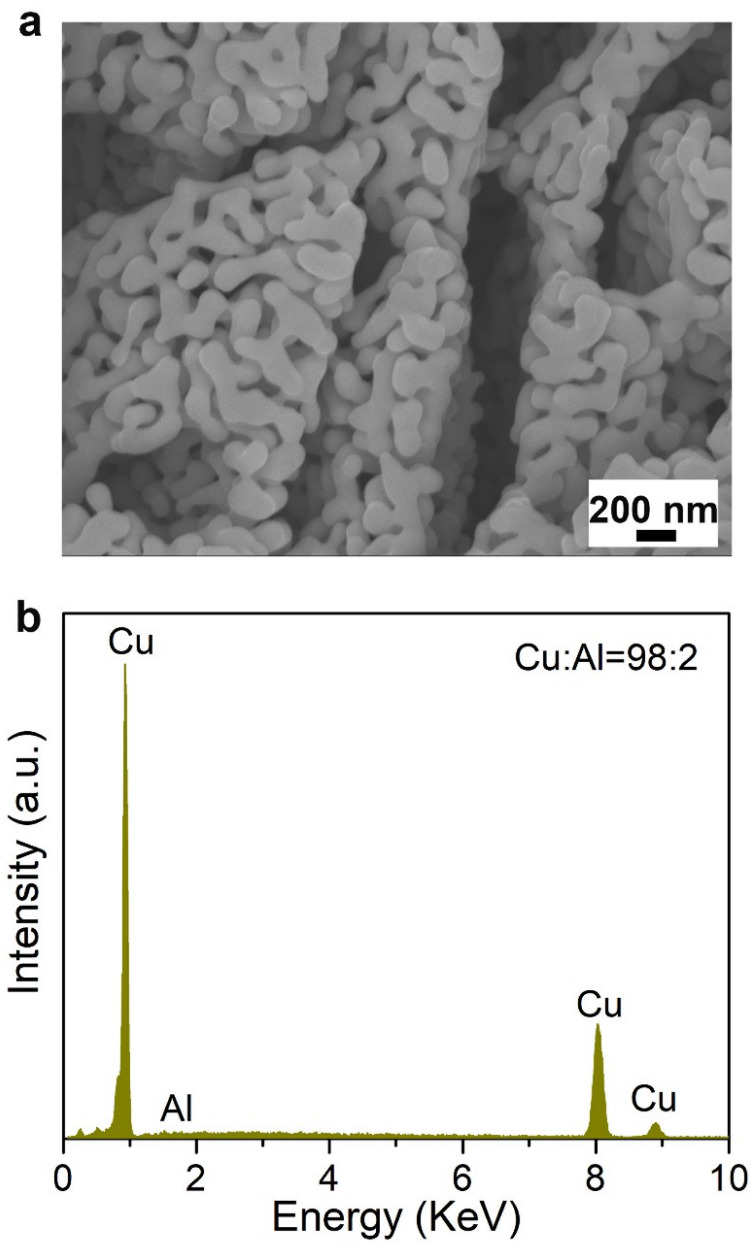

Fig. S5. (a, b) Typical SEM (a) and EDS spectrum (b) of nanoporous Cu electrode, which is fabricated by chemically dealloying $Cu_{15}Al_{85}$ alloy.

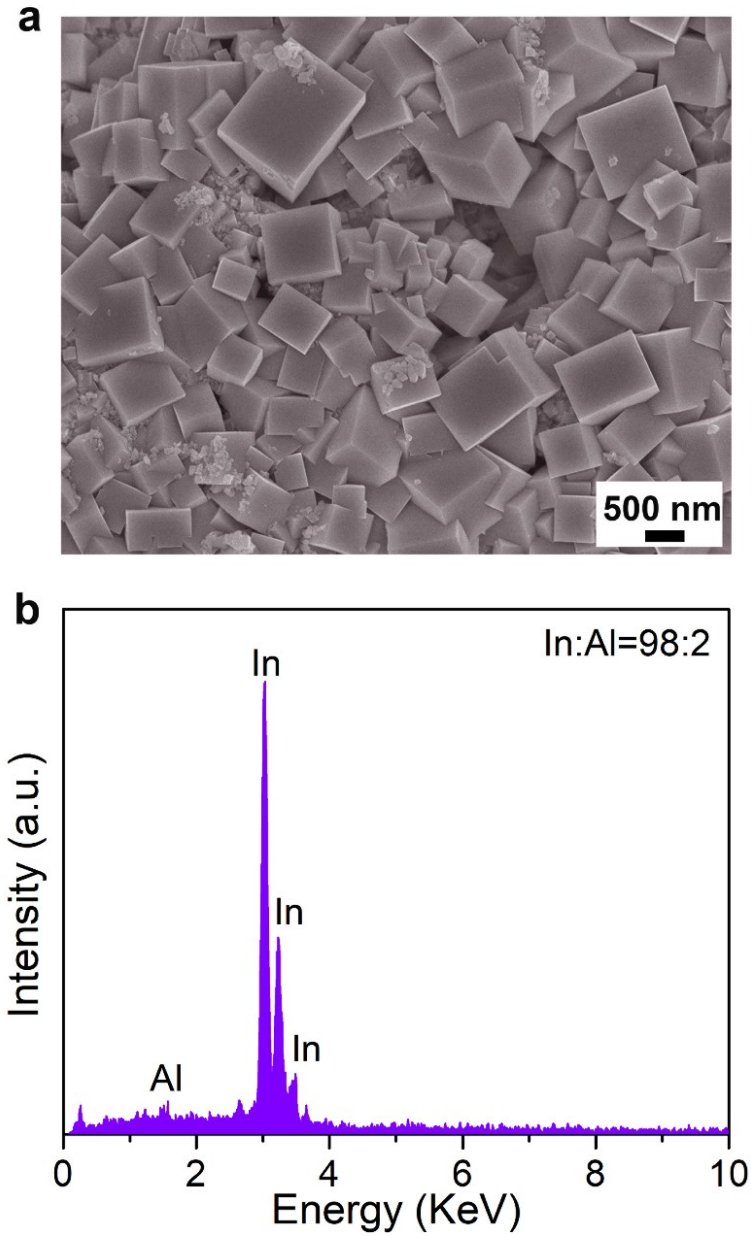

Fig. S6. (a, b) Typical SEM (a) and EDS spectrum (b) of $In(OH)_3$/In electrode, which is fabricated by chemically dealloying $In_{15}Al_{85}$ alloy.

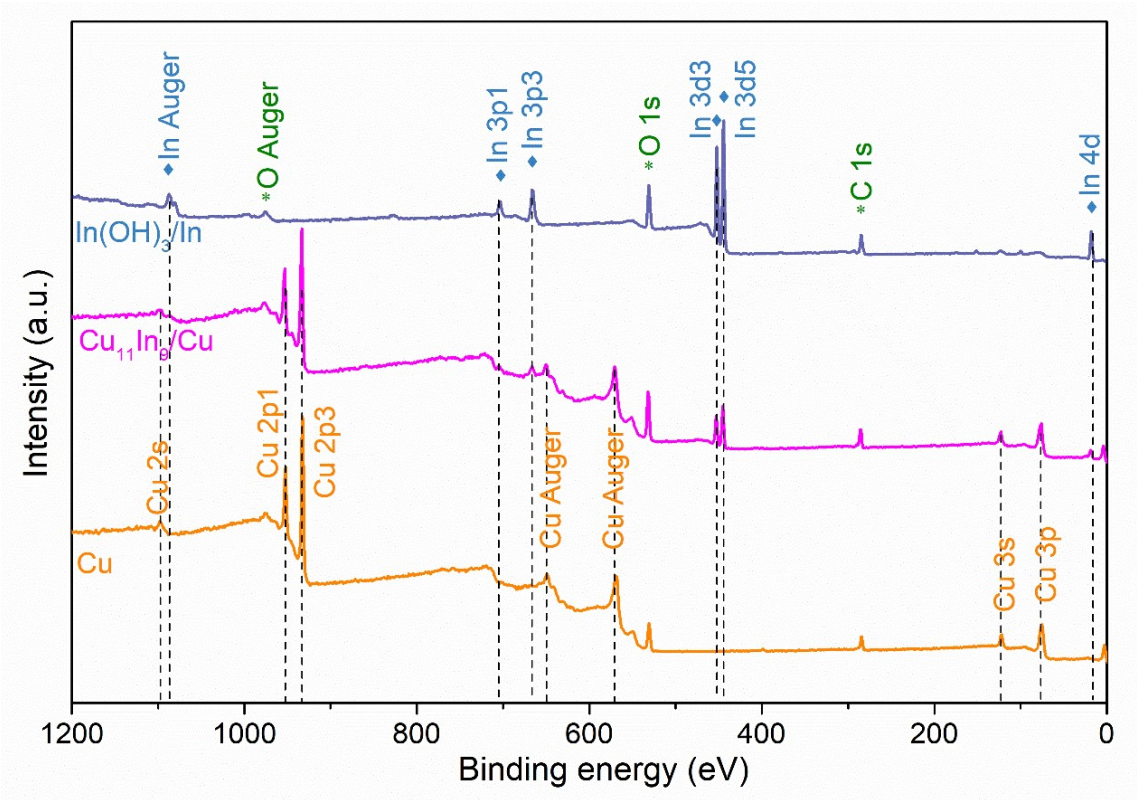

Fig. S7. XPS survey for nanoporous $Cu_{11}In_9$/Cu, nanoporous bare Cu and $In(OH)_3$/In, electrodes, which are prepared by chemically dealloying $Cu_{10}In_5Al_{85}$, $Cu_{15}Al_{85}$, and $In_{15}Al_{85}$ alloys, respectively.

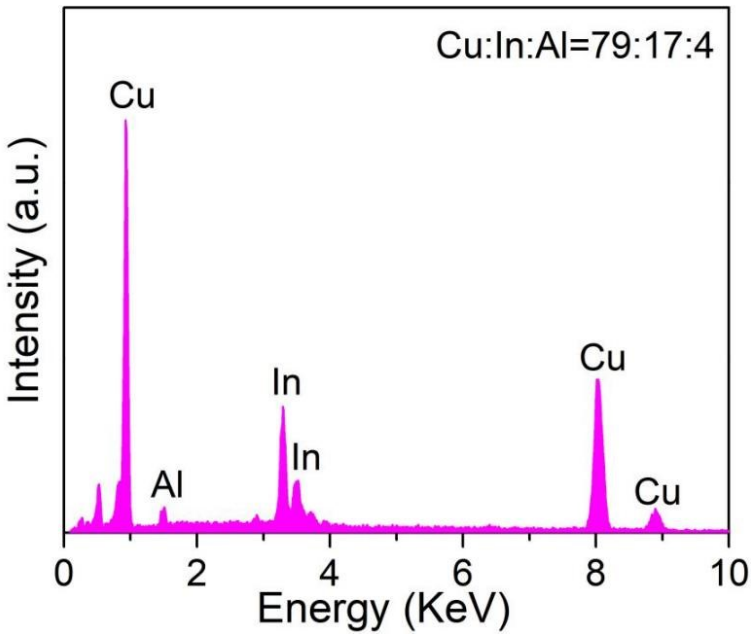

Fig. S8. EDS spectrum of as-dealloyed nanoporous $Cu_{11}In_9$/Cu hybrid electrode, which is prepared by chemically dealloying $Cu_{10}In_5Al_{85}$ alloy.

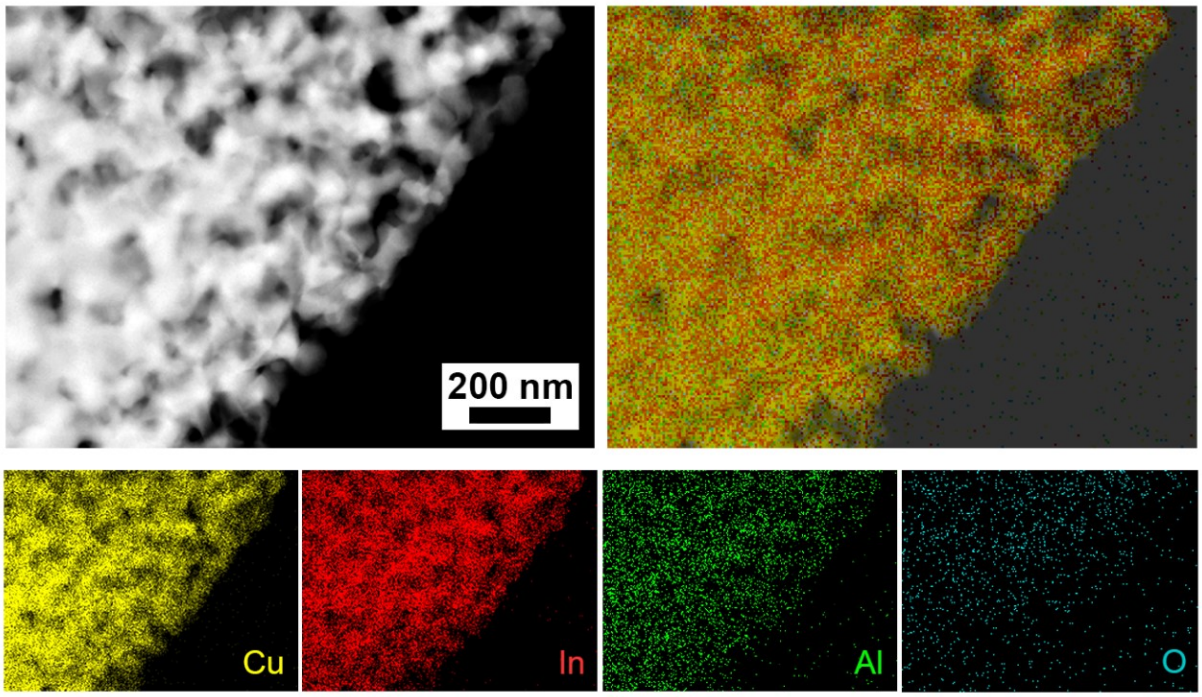

Fig. S9. STEM image of as-dealloyed nanoporous $Cu_{11}In_9$/Cu hybrid electrode and its corresponding STEM-EDS elemental mapping of Cu, In, Al and O.

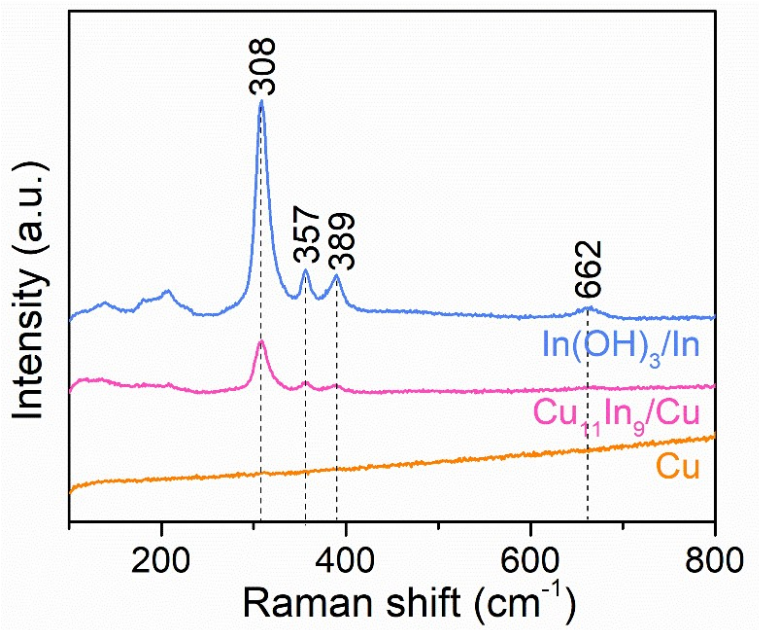

Fig. S10. Raman spectra of as-dealloyed nanoporous $Cu_{11}In_9$/Cu, nanoporous bare Cu, and $In(OH)_3$/In electrodes.

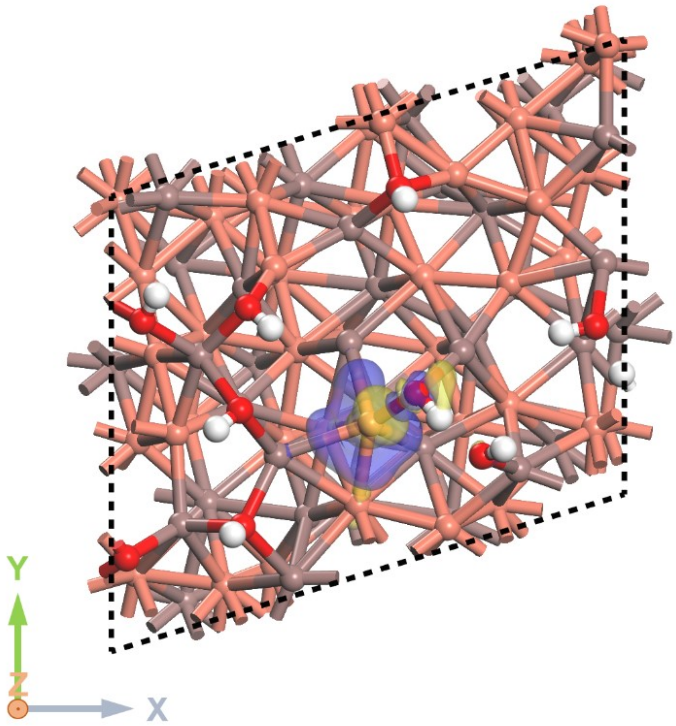

Fig. S11. The charge density difference diagram of Cu-In$(OH)_x$/$Cu_{11}In_9$(313) and the Hirshfeld charge analysis. The blue isosurfaces represent charge accumulation and the yellow represent charge depletion.

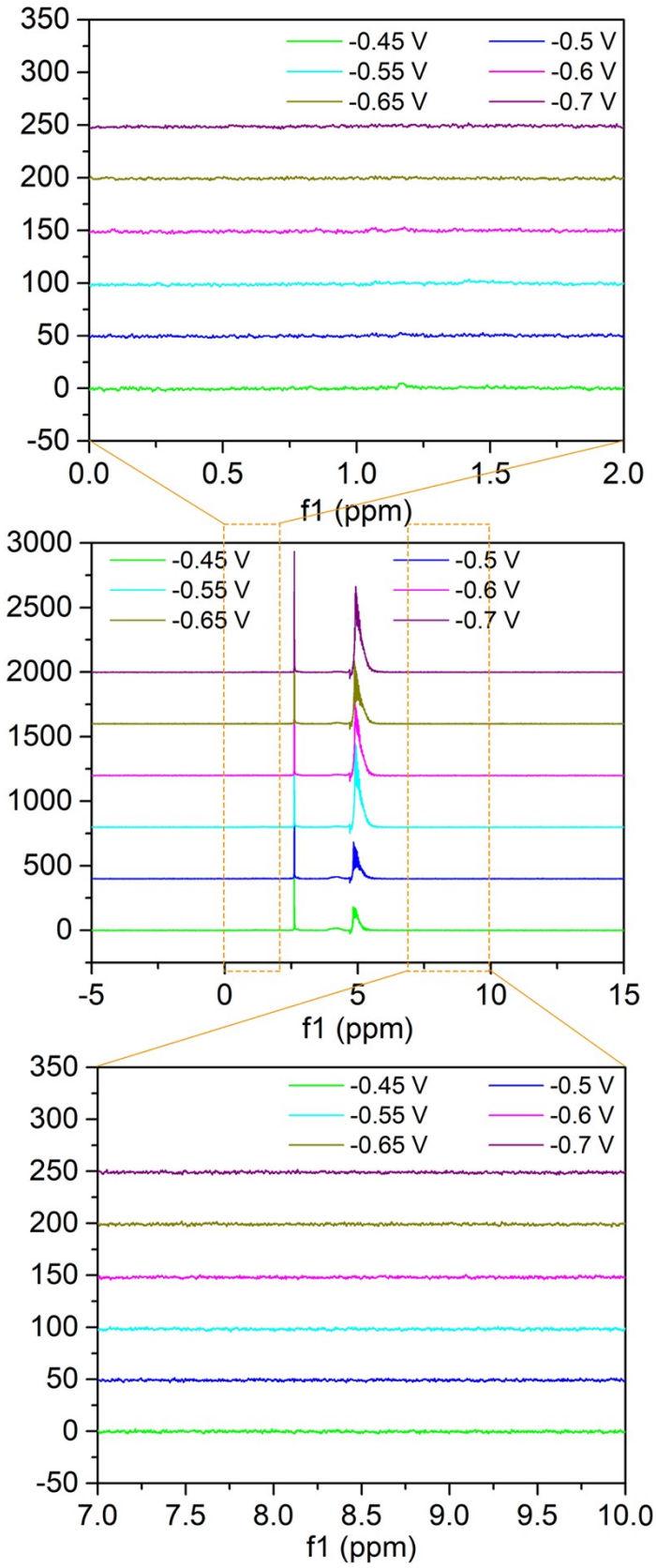

Fig. S12. Detection of liquid products of nanoporous $Cu_{11}In_9$/Cu hybrid electrode by 1 H nuclear magnetic resonance spectroscopy.

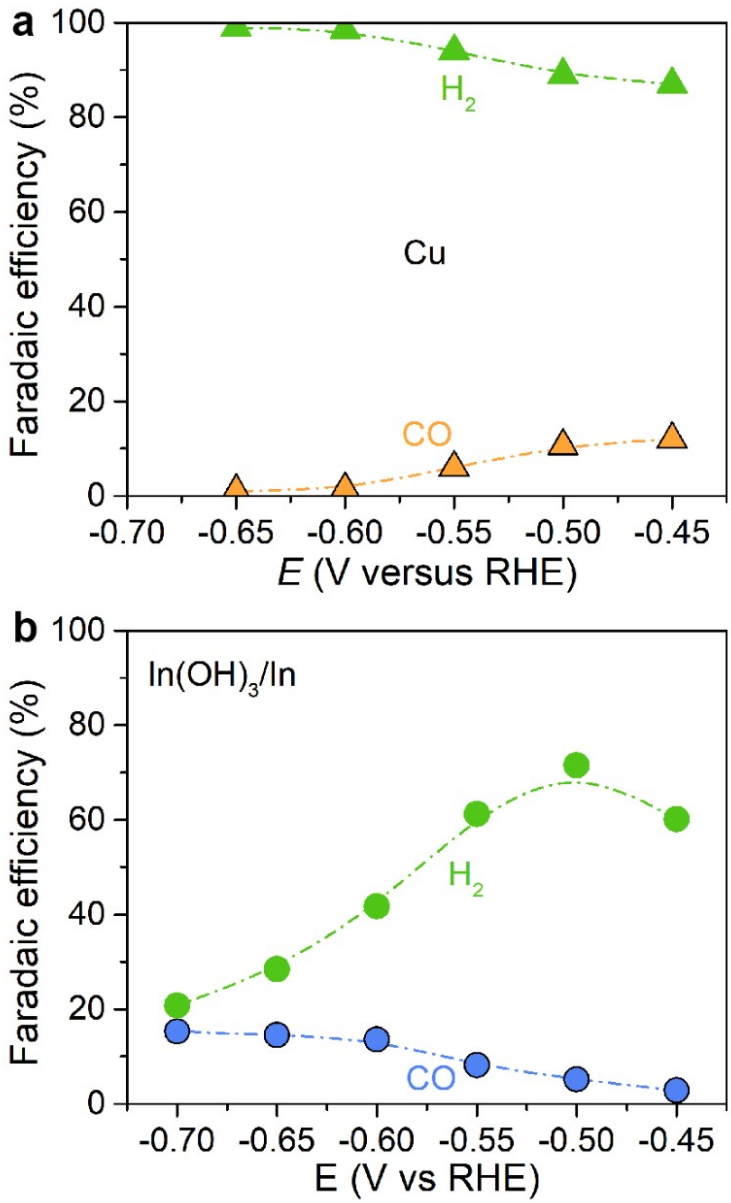

Fig. S13. (a) Faradaic efficiencies of CO and H_2 products during the CO_2 electroreduction of nanoporous bare Cu electrode in CO_2-saturated 0.1 M $KHCO_3$ solution at various potentials ranging from –0.45 to –0.65 V versus RHE. (b) Faradaic efficiencies of CO and H_2 products during the CO_2 electroreduction of $In(OH)_3$/In electrode in CO_2-saturated 0.1 M $KHCO_3$ solution at various potentials ranging from –0.45 to –0.70 V versus RHE.

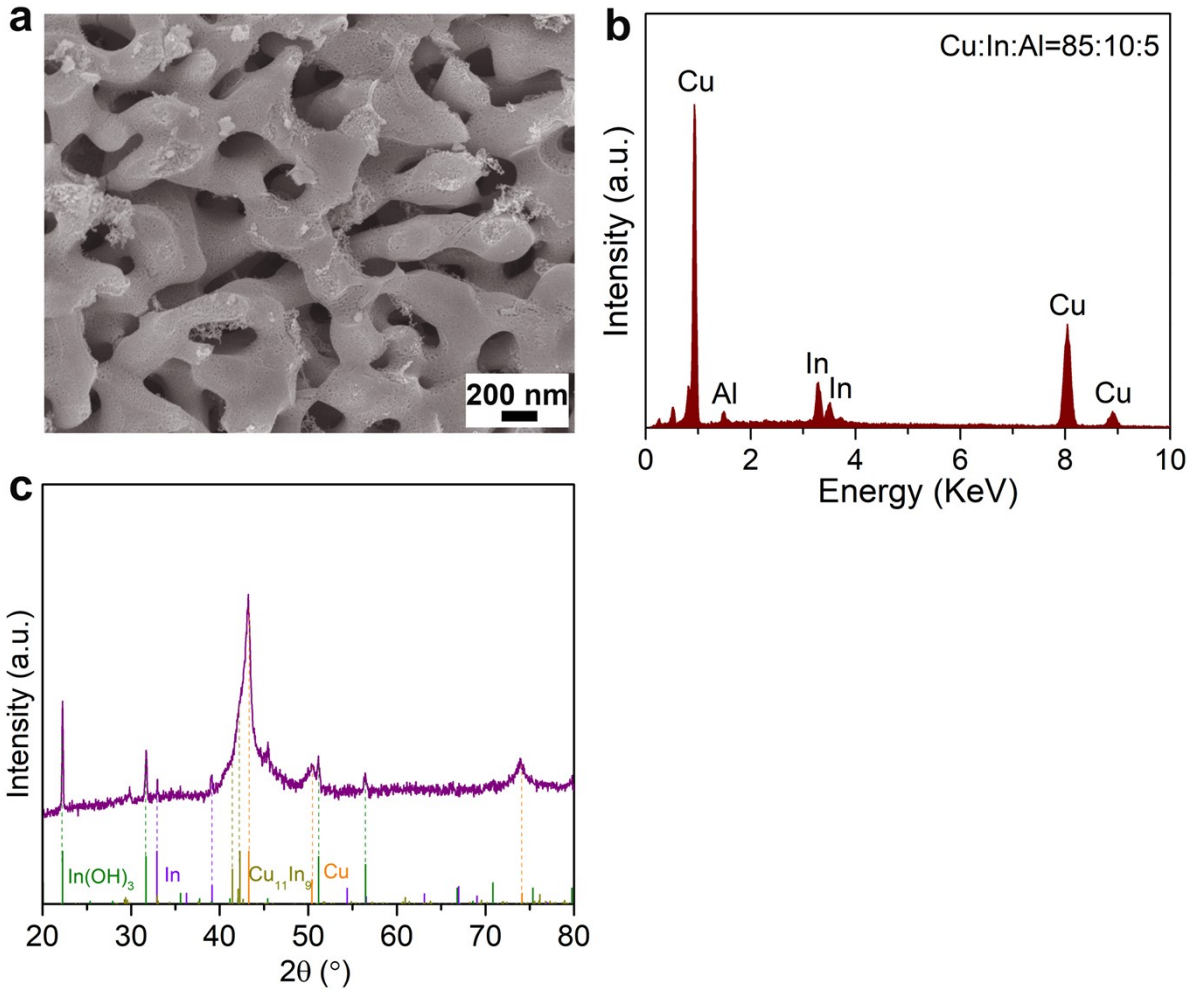

Fig. S14. (a) Typical SEM of as-dealloyed nanoporous $Cu_{11}In_9$/Cu from precursor $Cu_{12}In_3Al_{85}$ alloy. (b) EDS spectrum of as-dealloyed nanoporous $Cu_{11}In_9$/Cu from precursor $Cu_{12}In_3Al_{85}$ alloy. (c) XRD patterns of as-dealloyed nanoporous $Cu_{11}In_9$/Cu from precursor $Cu_{12}In_3Al_{85}$ alloy.

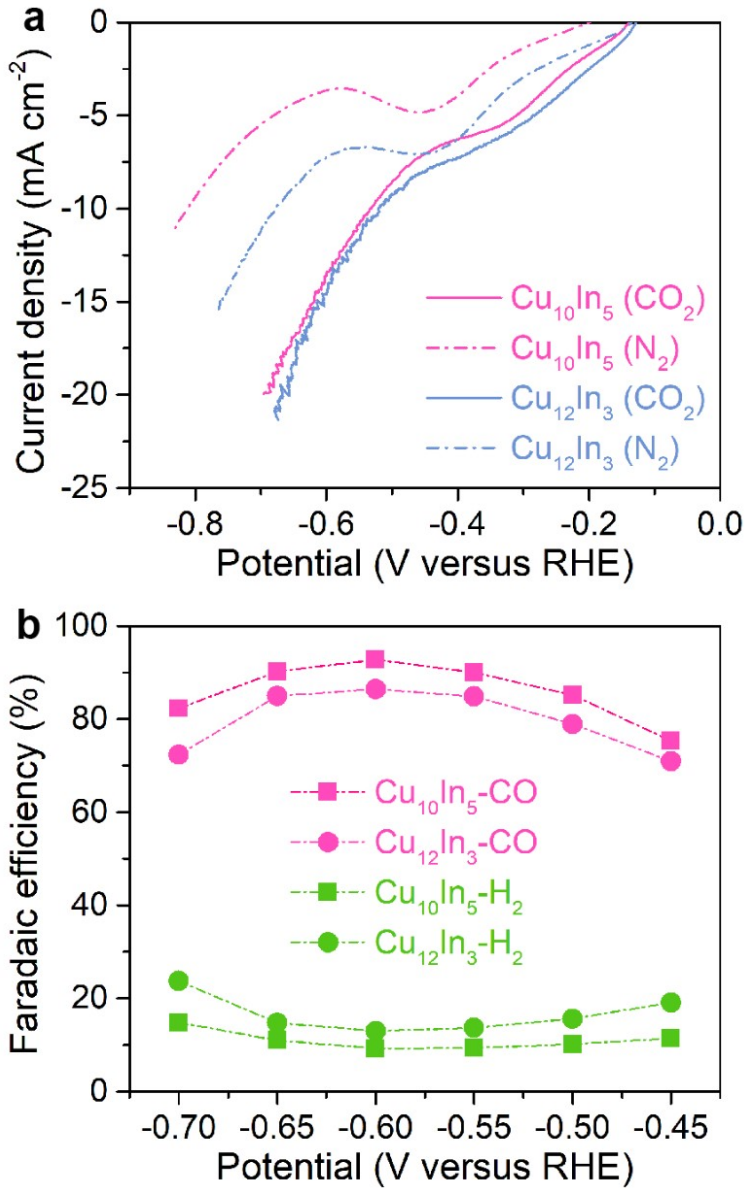

Fig. S15. (a) Comparison of LSV curves for as-dealloyed nanoporous $Cu_{11}In_9$/Cu hybrid electrodes from $Cu_{10}In_5Al_{85}$ and $Cu_{12}In_3Al_{85}$ precursor alloys, in 0.1 M N_2 and CO_2-saturated $KHCO_3$ solution. (b) Comparisons of Faradaic efficiencies of CO and H_2 products for nanoporous $Cu_{11}In_9$/Cu hybrid electrodes from $Cu_{10}In_5Al_{85}$ and $Cu_{12}In_3Al_{85}$ precursor alloys.

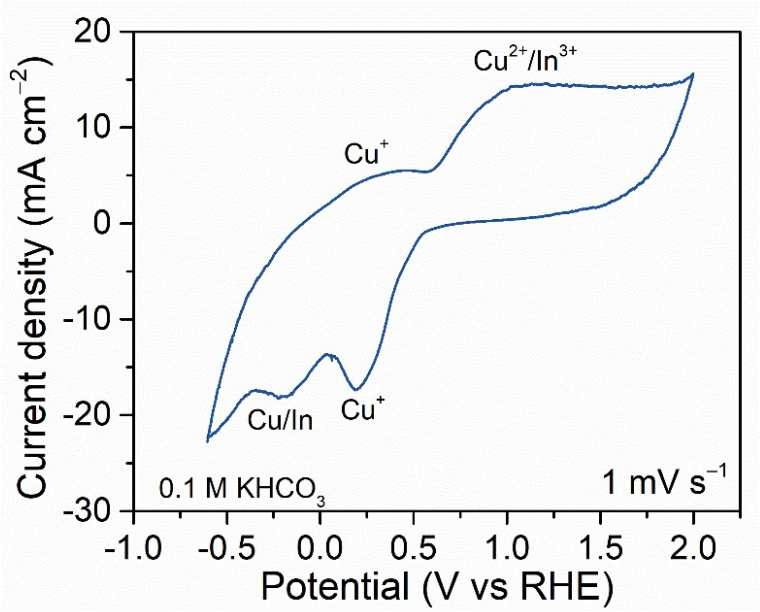

Fig. S16. Typical CV curve of as-dealloyed nanoporous $Cu_{11}In_9$/Cu from precursor $Cu_{10}In_5Al_{85}$ alloy in 0.1 M $KHCO_3$ solution. Scan rate: 1 mV s^{-1}.

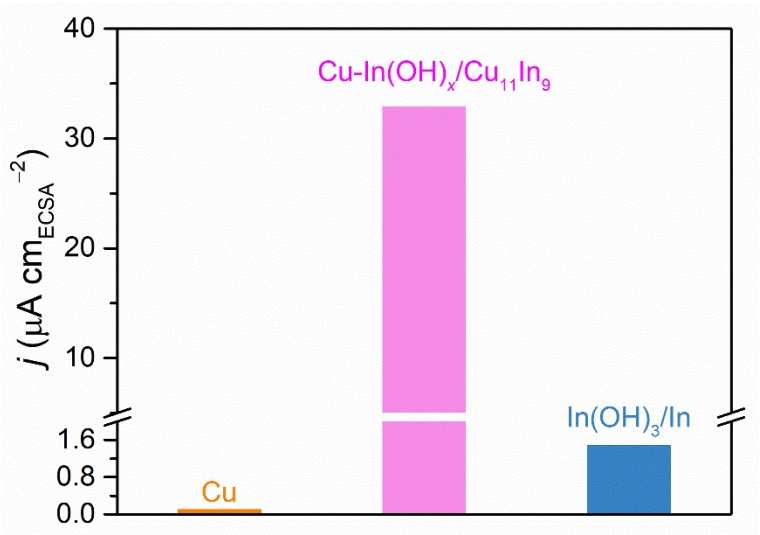

Fig. S17. Comparison of intrinsic activities for intermetallic Cu-In(OH)$_x$/Cu$_{11}$In$_9$, Cu and In(OH)$_3$ towards CO_2RR for CO product.

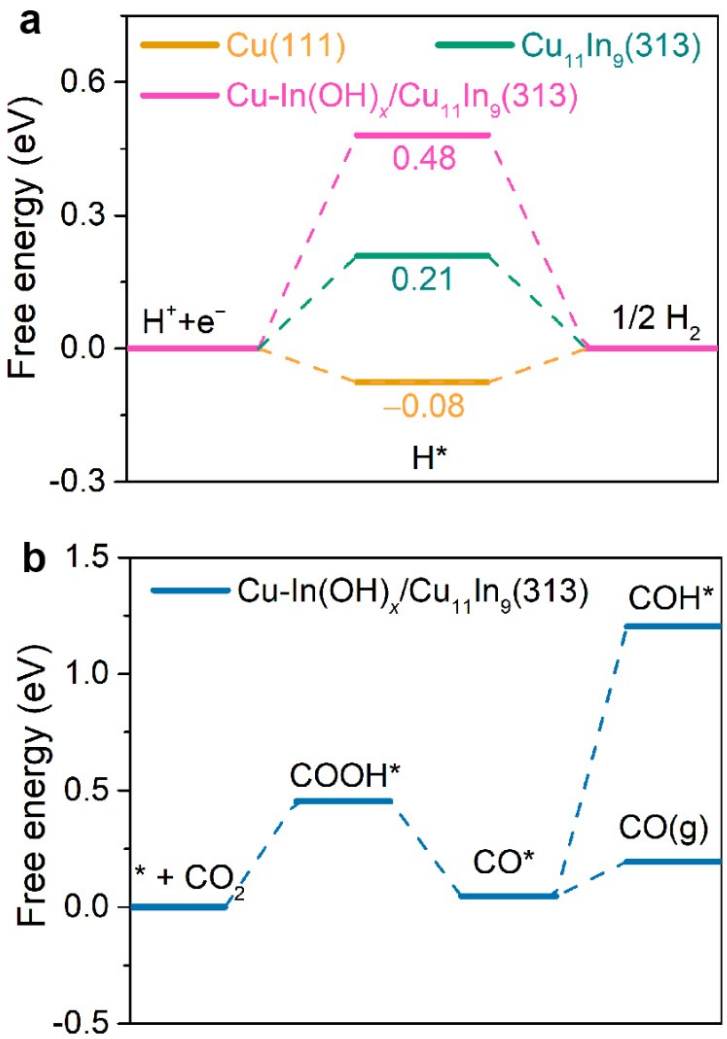

Fig. S18. (a) Free energies for the formation of H* on Cu-In(OH)$_x$/$Cu_{11}In_9$(313) and $Cu_{11}In_9$(313), Cu(111) surface. (b) Reaction free energy diagram for the CO_2 reduction with CO product or COH* intermediate from the adsorbed *CO_2 intermediate on intermetallic Cu-In(OH)$_x$/$Cu_{11}In_9$(313).

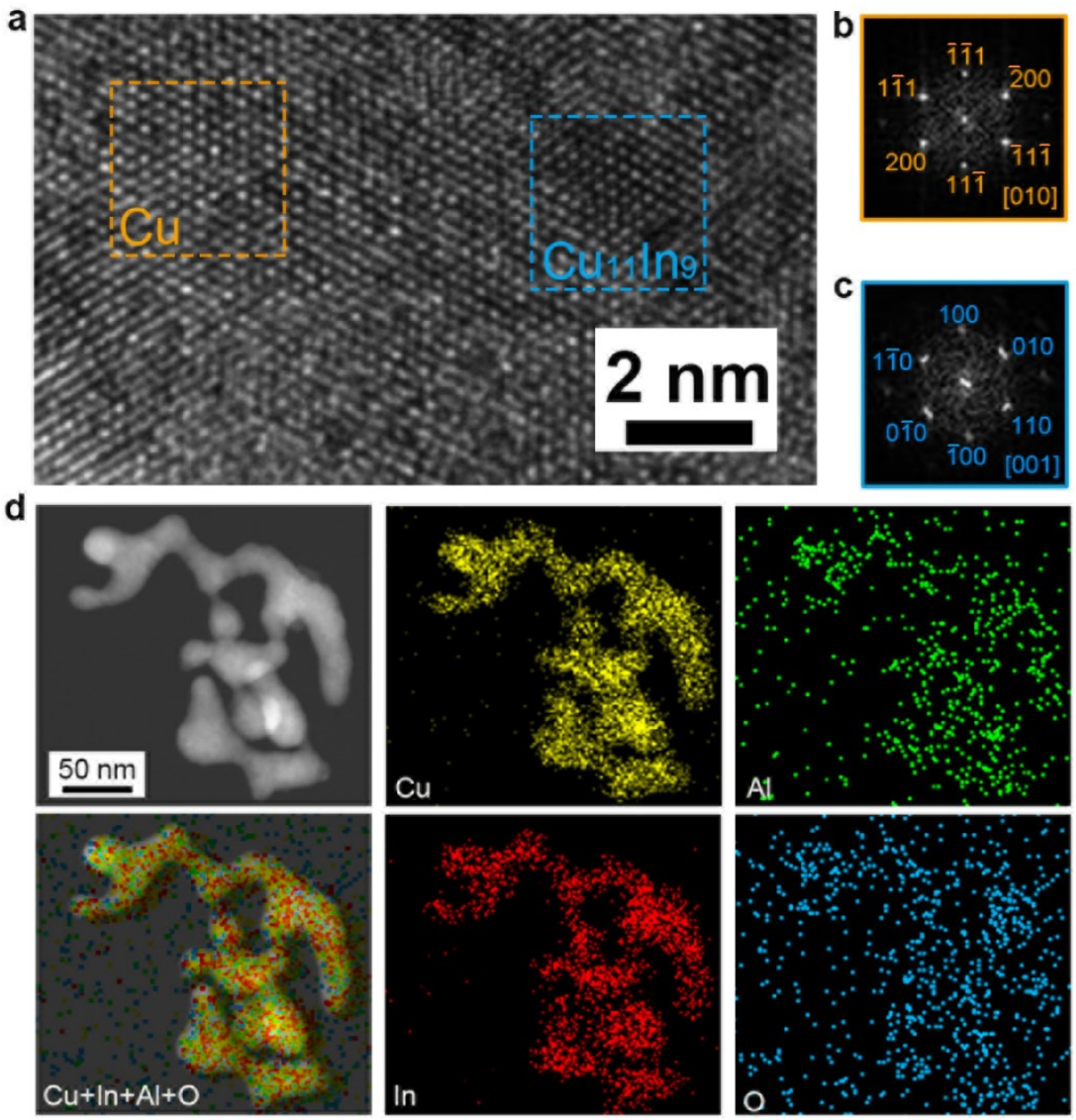

Fig. S19. (a) HRTEM image of $Cu_{11}In_9$/Cu interfacial region in nanoporous $Cu_{11}In_9$/Cu hybrid electrodes after the durability test, in which intermetallic $Cu_{11}In_9$ and FCC Cu matrix are identified by their corresponding FFT patterns. (b, c) FFT patterns of monoclinic $Cu_{11}In_9$ nanoparticles (b) and FCC Cu matrix (c) corresponding to the selected areas in (a). (d) STEM image and the corresponding STEM-EDS elemental mapping of Cu, In, Al and O in nanoporous $Cu_{11}In_9$/Cu hybrid electrode after the durability test.

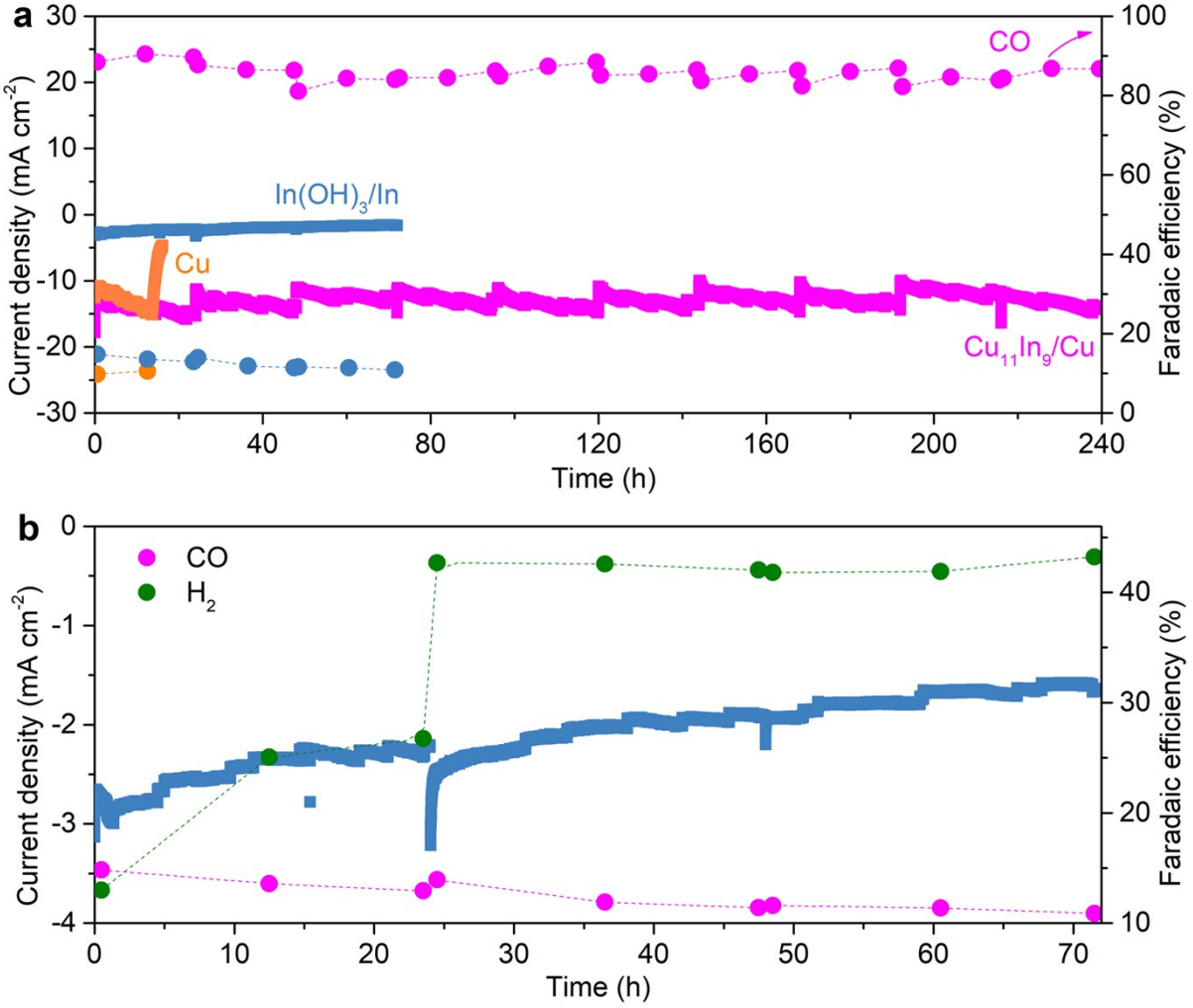

Fig. S20. (a) Comparison of the stability of nanoporous $Cu_{11}In_9/Cu$, nanoporous bare Cu and $In(OH)_3/In$ electrodes. (b) Magnification of the stability and Faradaic efficiencies of H_2 and CO for the $In(OH)_3/In$ electrode.

Table S1. Comparison of electrochemical parameters of nanoporous $Cu_{11}In_9/Cu$ with those of state-of-the-art metal-based CO_2RR catalysts previously reported in 0.1 M $KHCO_3$ aqueous electrolyte.

Electrocatalysts	Electrolyte	*E* (V vs RHE)	J_{CO} (mA cm^{-2})	FE_{CO}	R_{CO} (μmol h^{-1} cm^{-2})	Refs.
$Cu_{11}In_9/Cu$	0.1 M $KHCO_3$	-0.6	12.6	92.8%	235.1	This work
Zn P-NS	0.1 M $KHCO_3$	-1.2	13	90%	242.5	[1]
ZnO NS	0.1 M $KHCO_3$	-1.1	16.1	83%	300.4	[2]
Ni-N-C	0.1 M $KHCO_3$	-0.78	9 A g^{-1}	85%	/	[3]
Fe/NG-750	0.1 M $KHCO_3$	-0.6	2.5	80%	46.6	[4]
Pd nanoparticles	0.1 M $KHCO_3$	-0.89	4	91%	74.6	[5]
Fe-N-C	0.1 M $KHCO_3$	-1.0	3.2	80%	59.7	[6]
NCNTs	0.1 M $KHCO_3$	-1.05	3.8	80%	70.9	[7]
CuO+ALD SnO_2	0.1 M $KHCO_3$	-0.6	0.4	89%	7.5	[8]
NC-CNTs (Ni)	0.1 M $KHCO_3$	-0.8	7.2	91%	134.3	[9]
Tri-Ag-NPs Ag-NPs	0.1 M $KHCO_3$	-0.85 -0.85	1.25 0.6	95% 65%	23.3 11.2	[10]
Au-IO	0.1 M $KHCO_3$	-0.5	0.12	97%	2.2	[11]
Plasma-treated Ag	0.1 M $KHCO_3$	-0.6	2.1	90%	39.2	[12]
Au nanoparticles Au_3Cu	0.1 M $KHCO_3$	-0.9 -0.72	3.0 0.9	66% 65%	56.0 16.8	[13]
Au_3Cu@fct Au	0.1 M $KHCO_3$	-0.8	10	94.5%	186.5	[14]
Au_{55}/C	0.1 M $KHCO_3$	-0.6	4.7	94.1%	87.7	[15]
Fe-N-C	0.1 M $KHCO_3$	-0.6	12.5	95%	233.2	[16]
Cu-In	0.1 M $KHCO_3$	-0.6	0.9	90%	16.79	[17]
Cu-N_2/GN	0.1 M $KHCO_3$	-0.5	0.8	81%	14.9	[18]
Au_1Ni_1/CNFs	0.1 M $KHCO_3$	-0.98	4	92%	74.6	[19]
A-MnO_x-H	0.1 M $KHCO_3$	-0.62	10.4	94.8%	194.0	[20]
CN-H-CNT	0.1 M $KHCO_3$	-0.5	0.25	88%	4.7	[21]
CuIn20	0.1 M $KHCO_3$	-0.6	1.6	93%	29.8	[22]
BAX-M-950	0.1 M $KHCO_3$	-0.66	0.8	40%	14.9	[23]

NP Au-Zn	0.1 M $NaHCO_3$	-0.6	4.95	90%	92.3	[24]
Co_1-N_4	0.1 M $KHCO_3$	-0.8	11.25	82%	209.9	[25]
Cu-Pd NPs	0.1 M $KHCO_3$	-0.9	2.83	87%	52.8	[26]
Ag@Cu-7	0.1 M $KHCO_3$	-1.06	1.23	82%	22.9	[27]
Zn(101)	0.1 M $KHCO_3$	-0.9	5.4	45%	100.7	[28]
Cu-In alloy	0.1 M $KHCO_3$	-0.8	0.18	35%	3.4	[29]
WIT SnO_2	0.1 M $KHCO_3$	-0.89	1.71	38%	31.9	[30]
Pd Icosahedra/C	0.1 M $KHCO_3$	-0.8	1.9	91.1%	35.4	[31]
FePGH-H	0.1 M $KHCO_3$	-0.44	1.1	98%	20.5	[32]
Ni-CTF	0.1 M $KHCO_3$	-0.9	1.75	96%	32.6	[33]
Au foil	0.1 M $KHCO_3$	-1.0	2	35%	37	[34]

Table S2. ICP analysis of Cu and In ions in electrolyte before and after cycling measurement of nanoporous $Cu_{11}In_9$/Cu electrode.

	Cu (mg/L)	In (mg/L)
Original electrolyte	0.0468	0.0289
Electrolyte after recycling	0.0545	0.0348

Supplementary references

(1) K. Liu, J. Wang, M. Shi, J. Yan, Q. Jiang, *Adv. Energy Mater.* **2019**, *9*, 1900276.
(2) Z. Geng, X. Kong, W. Chen, H. Su, Y. Liu, F. Cai, G. Wang, J. Zeng, *Angew. Chem. Int. Ed.* **2018**, *130*, 6162.
(3) W. Ju, A. Bagger, C. P. Hao, A. S. Varela, I. Sinev, V. Bon, B. R. Cuenya, S. Kaskel, J. Rossmeisl, P. Strasser, *Nat. Commun*. **2017**, *8*, 944.
(4) C. Zhang, S. Yang, J. Wu, M. Liu, S. Yazdi, M. Ren, J. Sha, J. Zhong, K. Nie, A. S. Jalilov, Z. Li, H. Li, B. I. Yakobson, Q. Wu, E. Ringe, H. Xu, P. M. Ajayan, J. M. Tour, *Adv. Energy Mater.* **2018**, *8*, 1703487.
(5) D. Gao, H. Zhou, J. Wang, S. Miao, F. Yang, G. Wang, J. Wang, X. Bao, *J. Am. Chem. Soc.* **2015**, *137*, 4288.
(6) A. S. Varela, M. Kroschel, N. D. Leonard, W. Ju, J. Steinberg, A. Bagger, J. Rossmeisl, P. Strassre, *ACS Energy Lett.* **2018**, *3*, 812.
(7) P. P. Sharma, J. Wu, R. M. Yadav, M. Liu, C. J. Wright, C. S. Tiwary, B. I. Yakobson, J. Lou, P. M. Ajayan, X. D. Zhou, *Angew. Chem. Int. Ed.* **2015**, *127*, 13905.
(8) M. Schreier, F. Héroguel, L. Steier, S. Ahmad, J. S. Luterbacher, M. T. Mayer, J. Luo, M. Gratzel, *Nat. Energy* **2017**, *2*, 17087.
(9) Q. Fan, P. Hou, C. Choi, T. S. Wu, S. Hong, F. Li, Y. L. Soo, P. Kang, Y. Jung, Z. Sun, *Adv. Energy Mater.* **2020**, *10*, 1903068.
(10) S. Liu, H. Tao, L. Zeng, Q. Liu, Z. Xu, Q. Liu, J. L. Luo, *J. Am. Chem. Soc.* **2017**, *139*, 2160.
(11) A. S. Hall, Y. Yoon, A. Wuttig, Y. Surendranath, *J. Am. Chem. Soc.* **2015**, *137*, 14834.
(12) H. Mistry, Y. W. Choi, A. Bagger, F. Scholten, C. S. Bonifacio, I. Sinev, N. J. Divins, I. Zegkinoglou, H. S. Jeon, K. Kisslinger, E. A. Stach, J. C. Yang, J. Rossmeisl, B. R. Cuenya, *Angew. Chem. Int. Ed.* **2017**, *129*, 11552.
(13) D. Kim, J. Resasco, Y. Yu, A. M. Asiri, P. Yang, *Nat. Commun*. **2014**, *15*, 4948.
(14) D. Yu, L. Gao, T. Sun, J. Guo, Y. Yuan, J. Zhang, M. Li, X. Li, M. Liu, C. Ma, Q. Liu, A. Pan, J. Yang, H. Huang, *Nano Lett.* **2021**, *21*, 1003.
(15) X. K. Wan, J. Q. Wang, Q. M. Wang, *Angew. Chem. Int. Ed.* **2021**, *133*, 1.
(16) N. M. Adli, W. Shan, S. Hwang, W. Samarakoon, S. Karakalos, Y. Li, D. A. Cullen, D. Su, Z. Feng, G. Wang, G. Wu, *Angew. Chem. Int. Ed.* **2021**, *133*, 1035.
(17) S. Rasul, D. H. Anjum, A. Jedidi, Y. Minenkov, L. Cavallo, K. Takanabe, *Angew. Chem. Int. Ed.* **2015**, *127*, 2174.
(18) W. Zheng, J. Yang, H. Chen, Y. Hou, Q. Wang, M. Gu, F. He, Y. Xia, Z. Xia, Z. Li, B. Yang, L. Lei, C. Yuan, Q. He, M. Qiu, X. Feng, *Adv. Funct. Mater.* **2020**, *30*, 1907658.
(19) J. Hao, H. Zhu, Y. Li, P. Liu, S. Lu, F. Duan, W. Dong, Y. Lu, T. Liu, M. Du, *Chem. Eng. J.* **2021**, *404*, 126523.
(20) H. Han, S. Jin, S. Park, Y. Kim, D. Jang, M. H. Seo, W. B. Kim, *Nano Energy* **2021**, *79*, 105492.
(21) X. Cui, Z. Pan, L. Zhang, H. Peng, G. Zheng, *Adv. Energy Mater.* **2017**, *7*, 1701456.
(22) W. Luo, W. Xie, R. Mutschler, E. Oveisi, G. L. D. Gregorio, R. Buonsanti, A. Zütte, *ACS Catal*. **2018**, 8, 6571.
(23) W. Li, B. Herkt, M. Seredycha, T. J. Bandosz, *Appl. Catal. B-Environ*. **2017**, 207, 195.
(24) M. N. Hossain, Z. Liu, J. Wen, A. Chen, *Appl. Catal. B-Environ*. **2018**, 236, 483.

(25) Z. Geng, Y. Cao, W. Chen, X. Kong, Y. Liu, T. Yao, Y. Lin, *Appl. Catal. B-Environ*. **2019**, 240, 234.
(26) Y. Mun, S. Lee, A. Cho, S. Kim, J. W. Han, J. Lee, *Appl. Catal. B-Environ*. **2019**, 246, 82.
(27) Z. Chang, S. Huo, W. Zhang, J. Fang, H. Wang, *J. Phys. Chem. C* **2017**, 121, 11368.
(28) B. Qin, Y. Li, H. Fu, H. Wang, S. Chen, Z. Liu, F. Peng, *ACS Appl. Mater. Interfaces* **2018**, 10, 20530.
(29) Z. B. Hoffman, T. S. Gray, K. B. Moraveck, T. B. Gunnoe, G. Zangari, *ACS Catal*. **2017**, 7, 5381.
(30) L. Fan, Z. Xia, M. Xu, Y. Lu, Z. Li, *Adv. Funct. Mater*. **2018**, 28, 1706289.
(31) H. Huang, H. Jia, Z. Liu, P. Gao, J. Zhao, Z. Luo, J. Yang, J. Zeng, *Angew. Chem. Int. Ed*. **2017**, 129, 3648.
(32) J. Choi, J. Kim, P. Wagner, S. Gambhir, R. Jalili, S. Byun, S. Sayyar, Y. M. Lee, D. R. MacFarlane, G. G. Wallace, D. L. Officer, *Energy Environ. Sci*. **2019**, 12, 747.
(33) P. Su, K. Iwase, T. Harada, K. Kamiya, S. Nakanishi, *Chem. Sci*. **2018**, 9, 3941.
(34) Y. Fang, J. C. Flake, *J. Am. Chem. Soc*. **2017**, 139, 3399.